

We are IntechOpen, the world's leading publisher of Open Access books Built by scientists, for scientists

6,900

Open access books available

186,000

International authors and editors

200M

Downloads

Our authors are among the

154

Countries delivered to

TOP 1%

most cited scientists

12.2%

Contributors from top 500 universities



WEB OF SCIENCE™

Selection of our books indexed in the Book Citation Index
in Web of Science™ Core Collection (BKCI)

Interested in publishing with us?
Contact book.department@intechopen.com

Numbers displayed above are based on latest data collected.
For more information visit www.intechopen.com



Research on Hydrogen-Bonded Materials Using Terahertz Technology

Kei Takeya and Kodo Kawase

Additional information is available at the end of the chapter

<http://dx.doi.org/10.5772/67640>

Abstract

We measured terahertz (THz) characterization of hydrogen-bonded materials using THz time domain spectroscopy (TDS) with a gas-cooling cryostat. The temperature and frequency dependencies of the complex dielectric constants of icy materials were measured over a wide temperature range. We checked the dielectric parameters of ices and gas hydrates using a mathematical model. Ice exhibits increasing absorption with frequency in the THz range because of the low-frequency tail of the infrared-absorption band. This behavior is also observed in gas hydrates. The parameters describing the frequency dependence of ϵ'' are treated as functions of temperature. From the THz spectroscopy on gas hydrates, we showed that the dielectric constants of the gas hydrates in the THz range can be analyzed using methods for ice. The complex dielectric constants in the THz range contribute to the infrared polarization and phonon absorption of the water molecules on the hydrogen-bonding matrices, so we suggest that THz-TDS is useful for physical and chemical studies of gas hydrates.

Keywords: terahertz time domain spectroscopy, ice, gas hydrate

1. Introduction

A hydrogen bond is an interaction between two electronegative atoms through one hydrogen atom. The famous material as a crystal which consists of a hydrogen bond is an ice. Each oxygen atom in the structure of the ice is bonded to four oxygen atoms which are arranged as a tetrahedral around the oxygen atom through the hydrogen atom. Whereas materials which consist of the hydrogen bond contain the bond partially, ice is composed of only the hydrogen bond. The hydrogen bond is the controlling factor of the character of the ice [1]. Gas hydrates also consist of hydrogen bonds.

Gas hydrates have a curious icy crystalline structure which is stabilized under conditions of relatively high pressure and low temperature. Gas hydrates have attracted much attention as new materials for their use in the transport and storage of natural gases (**Figure 1**), since their structure contains high volume of gases. In particular, methane hydrate is abundant in many locations; it is found in sediment or permafrost regions and is expected to be a future energy resource. The structure of gas hydrates consists of many cages, which include guest gas molecules. Several structures of gas hydrates have been reported. The typical structure types are structures I, II, and H, and the type depends on the guest molecule size and temperature-pressure region. Structures I and II have a cubic unit cell, while structure H has a hexagonal cell. In structure-II hydrate, sixteen 12-Hedra cages (S-cages) and eight 16-Hedra cages (L-cages) are present in the unit cell. Structure I is generated by molecules with sizes 0.4–0.6 nm, while structure II is formed by somewhat larger (0.6–0.7 nm) molecules that occupy only the L-cages, such as tetrahydrofuran (THF) and propane. At high pressures, some of the smallest guest molecules (0.38–0.42 nm) such as argon or nitrogen form a structure-II hydrate and occupy both the S- and the L-cages. If the L-cages with structure II are fully occupied by compound A, the composition of the gas hydrate will be $A \cdot 17H_2O$ [2, 3].

Although ice and gas hydrates are important material for our life, several characters and phenomena are still unknown. The examples are as follows: the highest density of water at 4°C and the self-preservation effect of methane hydrate at around 250 K.

The stability, cage occupancy, structure, and other properties of gas hydrates have been investigated using Raman spectroscopy, X-ray diffraction, NMR, and so on [4–9]. The dielectric constants, which are fundamental parameters of a material, provide information on the water reorientation and proton disorder of the crystalline lattice of a hydrogen-bonded material. Although the dielectric parameters of ice have been reported in detail for a wide frequency and temperature range [1, 10–21], there are few such studies for gas hydrates. Davidson et al. provided a systematic discussion of the relaxation and reorientation of water molecules of gas hydrates using dielectric parameters [22–24]. Williams et al. reported measurements of the dielectric parameters to determine the dipole dispersion of guest molecules [25, 26]. Rick and Freeman reported a computational study of the proton disorder of structure-II hydrates using



Figure 1. Burning methane hydrates.

dielectric parameters [27]. These studies were conducted for frequencies below GHz frequencies, and there are few studies of gas hydrates at higher frequencies in the terahertz (THz) region [28, 29]. The frequency-dependent dielectric constants of the hydrogen-bonded materials provide information on the hydrogen-bonded structures.

In terms of the dielectric constant, the real part of the dielectric constant below 10^4 Hz of ice is dominated by orientation polarization, and the value beyond around 10^5 Hz is dominated by ionic polarization. The value drops from 3.2 to 1.7 at around a few THz, that is, the region of infrared absorption. In the region between a few THz and deep ultraviolet, electronic polarization dominates the value of the dielectric [30]. Hence, a study of the dielectric parameter at THz frequency is able to investigate the nature of the hydrogen-bonded structure. The above studies have mainly reported in the case of ice, whereas the report for the gas hydrate is not sufficient. Further, the report of the dielectric parameter at THz region is not sufficient.

THz region lies between the optical region and microwave region. The energy of a THz wave corresponds to the motion of a relatively large molecule; thus, THz waves offer the ability to observe absorption of a highly polymerized compound [31]. The energy is also related to the rotation of a hydrogen bond of water molecules and the rotation of free water molecules [32], so THz waves have the potential to observe water dynamics in a solution. Although it has been difficult to use THz waves due to the lack of a good emitter to date, recent developments in the technology of THz emitters and detectors have allowed many applications of THz technology, such as security checks, communications, nondestructive inspection, and spectroscopy [33, 34].

Famous for one of the THz applications is the THz time domain spectroscopy (TDS). THz-TDS is a convenient analytical technique that allows one to determine the optical constants and absorption coefficients of samples without using the Kramers-Kronig relationship [35]. Several studies on water and ice using THz spectroscopy have been reported so far [14, 36]. However, the temperature range used in these studies was very limited. The optical and dielectric properties of ice over a wide temperature range are expected to provide meaningful information for the fields of astronomy, remote-sensing, and low-temperature science. Ice in the proximity of a celestial body or in space exists at very low temperatures [1, 37–40]; moreover, ice in the low-temperature range exhibits interesting phenomena, such as an amorphous structure associated with the glass transition temperature [41, 42]. This information is necessary for THz remote-sensing applications. The frequency and temperature-dependent dielectric constants of ice provide information on hydrogen-bonded structures. Therefore, a survey of the optical parameters of hydrogen-bonded materials over a wide temperature range is necessary.

2. Research methods

For the preparation of water ice samples, we used ultrapure water and pure heavy water (WAKO Chemical). The water was placed in a Teflon plate with 10-mm-diameter holes to form tablet samples. The water and heavy water were frozen using an environmental testing

machine. The freezing of the water was slow and occurred at a temperature of 272 K to avoid mixing air bubbles into the ice. The tablet thickness ($\sim 1.0 \pm 0.005$ mm) was measured using a micrometer (Anritsu). The volume density of the tablet sample was over 99%, according to the volume and weight.

Propane and tetrahydrofuran (THF) hydrates were synthesized by stirring THF + water solution or pressurized gas and distilled water at 275.2 K in a stainless steel cell [28]. After stirring, the hydrates were extracted from the stainless cell at ca. 253 K in a low-temperature chamber. The obtained hydrate particles were crushed by the mortar and the pestle. The hydrate crystals were made into tablets with a diameter of 10 mm and varying thicknesses (1–2 mm) by using the tablet-making apparatus (Ichihashi-Seiki, HANDTAB-Jr) in the low-temperature chamber. The thickness of each sample was accurately calculated from the weight and the volume of water after melting. The error in the thickness is within 0.5%.

The tablet samples were measured using a THz-TDS system equipped with a dipole-type low-temperature-grown GaAs (LT-GaAs) photoconductive switch as an emitter and a detector and a Ti:sapphire laser (Mai-Tai, Spectra-Physics; $\lambda = 780$ nm; repetition rate: 82 MHz; pulse width: 100 fs) as a femtosecond pulsed laser source. The femtosecond laser pulse is first separated into a “pump pulse” and a “trigger pulse.” The THz pulse is generated at the photoconductive switch by the pump-pulse illumination and collimated onto the sample by using a set of off-axis parabolic mirrors and then collimated again onto the photoconductive switch antenna detector using another set of off-axis parabolic mirrors. Since the temporal photocurrent is generated only when the triggered laser pulse and the radiated THz pulse simultaneously arrive at the photoconductive switch, we can directly obtain both the amplitude and the phase of the radiated THz pulse by changing the optical delay and measuring the corresponding change in the photocurrent.

For the low-temperature measurement, a gas-cooled cryostat made by PASCAL was used. The temperature of the sample enclosure in the cryostat was maintained in the temperature range of 20–240 K using compressed He. The sample enclosure, equipped with quartz windows for transmitting THz waves, was positioned in the intermediate focal plane between the two sets of parabolic mirrors. The ice tablets were held at the top of a sample rod placed in the center between optical windows. During the initial sample setting, the sample rod was cooled by liquid nitrogen. The temperature distribution of the sample enclosure was kept uniform by circulating the helium cooling gas. Three thermistors surrounded the sample rod to monitor and maintain the set sample temperature within ± 0.2 K. All measurements were done multiple times, and each data is an averaged value.

The real and imaginary parts of the complex refractive indices, $n(\omega)$ and $k(\omega)$, of the samples can be directly calculated from the following equations:

$$\frac{E_{\text{sam}}(\omega)}{E_{\text{ref}}(\omega)} = \rho(\omega) \exp[-i\phi(\omega)] \quad (1)$$

$$n(\omega) = \frac{c\phi(\omega)}{\omega L} + 1 \quad (2)$$

$$k(\omega) = \frac{c}{\omega L} \ln \left\{ \frac{4n(\omega)}{\rho(\omega)[n(\omega) + 1]^2} \right\} \quad (3)$$

where ω is the frequency, $E_{\text{sam}}(\omega)$ is the fast Fourier transform (FFT) spectrum of the THz pulse propagating through the samples, $E_{\text{ref}}(\omega)$ is the reference FFT spectrum, $\rho(\omega)$ is the transmission, $\varphi(\omega)$ is the phase shift, c is the light speed, and L is the thickness of the sample [35]. Using these estimated complex refractive indices, we can obtain the real ϵ' and imaginary ϵ'' dielectric constants of the samples, as follows:

$$\epsilon'(\omega) = [n(\omega)]^2 - [k(\omega)]^2 \quad (4)$$

$$\epsilon''(\omega) = 2n(\omega)k(\omega) \quad (5)$$

3. Dielectric parameters of water ice and heavy water ice

The frequency dependence of the real part of the dielectric constants ϵ' of ice and heavy water ice is shown in **Figure 2**. Both ices were measured over the frequency range of 0.2–1.4 THz at 20, 100, 200, and 240 K. As the frequency increased from 0.2 to 1.4 THz, ϵ' increased from 3.12 to 3.24 for water ice and from 2.96 to 3.07 for heavy water ice at 200 K. The data expressed by open squares in **Figure 2(a)** are calculated, and values obtained from the reported complex index of refraction are shown in Ref. [14]. Our experimental data shows good agreement with the reported data at the same temperature. Lattice vibrations of the hydrogen-bonded water molecules contributed significantly to the amplitude of ϵ' in the THz frequency range [14]. The dielectric constant of heavy water ice is lower than that of water from comparison of both results. This is caused by a difference of polarization in water or heavy water ice. The polarization in heavy water ice is smaller than that in water ice, since a deuterium atom is heavier than hydrogen atom.

According to previous studies, the ϵ' values for ice are constant from 0.1 MHz to 1 THz and show complicated behavior beyond 1 THz, with the maximum occurring at a few THz [10, 19, 37]. The frequency range of our measurements corresponded to the range used in these

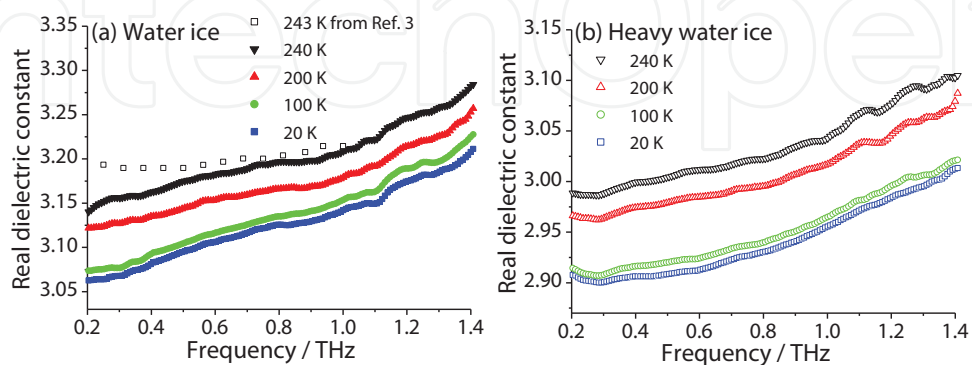


Figure 2. Frequency dependence of the real dielectric constant ϵ' of (a) water and (b) heavy water ice at 20, 100, 200, and 240 K. The reported data of water ice [14] are plotted in graph (a).

previous studies; thus, in our measurements, it was expected we observe a local maximum value for ϵ' of ice at several THz [10].

Figure 3 shows the temperature dependence of the real dielectric constant ϵ' for both ices at 0.26, 0.50, 0.75, and 1 THz. As the temperature increased from 10 to 240 K, ϵ' increased from 3.14 to 3.21 for water ice and from 2.95 to 3.04 for heavy water ice at 1 THz.

In previous reports of ϵ' of ice in the GHz regime, the temperature dependence of ϵ' has been discussed with regard to the contribution of inharmonic effects to the molecular polarizability α of lattice water [10, 12]. We can obtain α for water and heavy water ice in the THz frequency range using the Clausius–Mossotti equation:

$$\frac{N_i}{3} \alpha = \left(\frac{\epsilon' - 1}{\epsilon' + 2} \right) \quad (6)$$

where N_i is the number of molecules per unit volume. According to previous reports, the density for ice is 0.917 Mgm^{-3} ; for heavy water ice, it can be estimated as 1.019 Mgm^{-3} . The estimated values of α are 41.51 \AA^3 for water ice and 39.67 \AA^3 for heavy water ice at 1 THz at a temperature of 240 K (**Figure 4**). The values of heavy water ice are lower than those for water ice under the same conditions. This resulted from the mass of deuterium atoms. The molecular polarizability α is the sum of the electronic polarizability α_{el} (displacement of the molecules within the lattice) and the infrared polarizability α_{IR} (the vibration of the molecules within the lattice).

For ice, α_{el} is independent of temperature; thus, the temperature dependence of α appears in the α_{IR} term. Additionally, the α_{IR} of ice increases linearly with the square of the temperature (T^2) [10, 12]. Applying this discussion of the polarizability of ice to the present results, we derived the following equation for the molecular polarizability α :

$$\alpha = \alpha_{\text{el}} + \alpha_{\text{IR}} = \alpha_{\text{el}} + \alpha_{0,\text{IR}} + aT^2 \quad (7)$$

where $\alpha_{0,\text{IR}}$ is the infrared polarizability at 0 K and a is an empirical constant. Using Eq. (7), we determined that the fitted curves were in good agreement with the experimental results

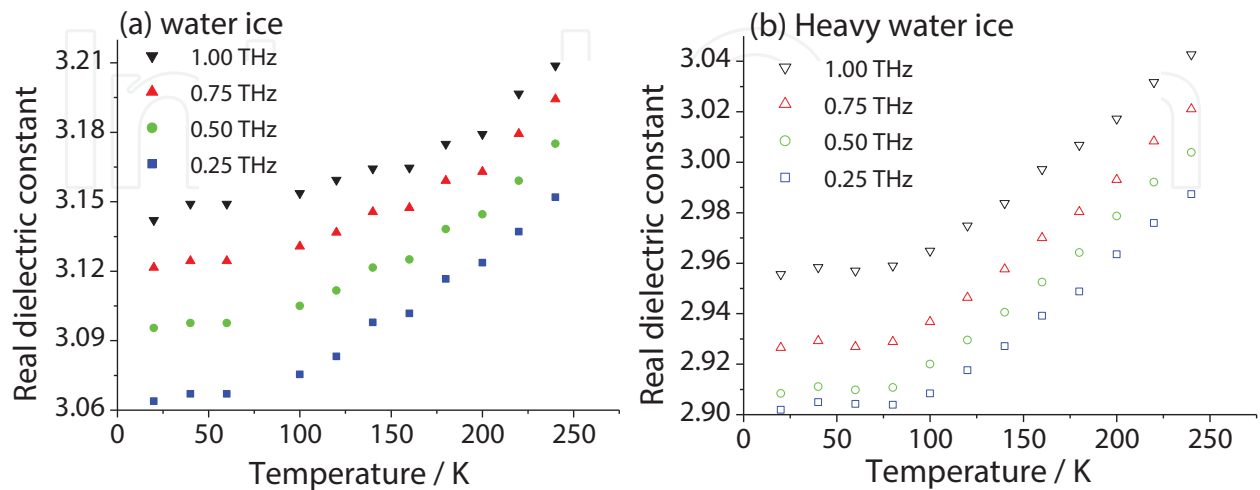


Figure 3. Temperature dependence of the real dielectric constant ϵ' at 0.25, 0.50, 0.75, and 1 THz for (a) water ice and (b) heavy water ice.

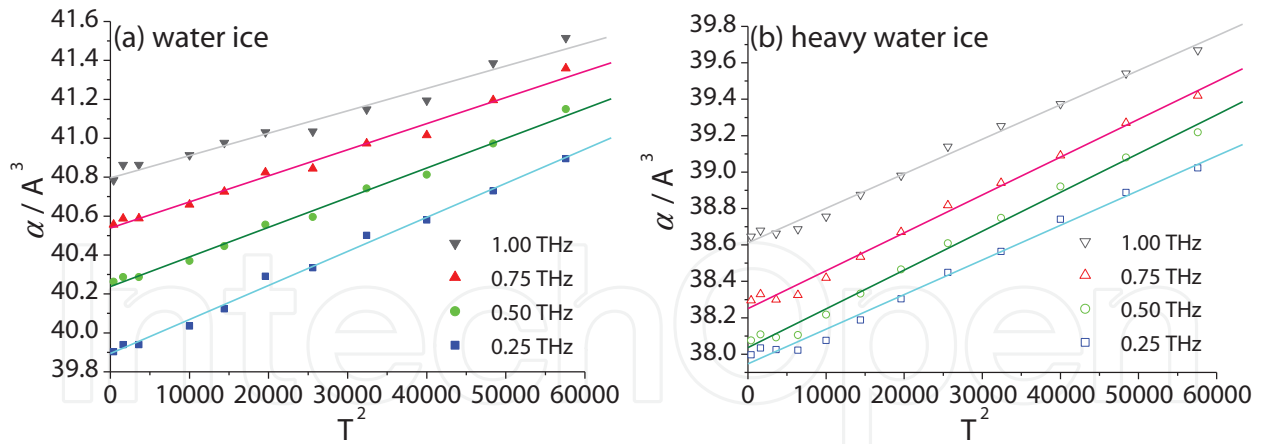


Figure 4. Molecular polarizability α of (a) water and (b) heavy water ice plotted versus temperature squared. The solid lines are the fitted curves obtained from Eq. (7) at 0.25, 0.50, 0.75, and 1.00 THz.

(Figure 4). The values of $\alpha_{el} + \alpha_{0,IR}$ and a derived from the fitted curves (Figure 4) are listed in Table 1. The value of a in the range of 0.26–0.75 THz was $\sim 8.6 \times 10^{-6}$, which was nearly constant, but it increased beyond 0.75 THz. The real dielectric constant ϵ' of ice exhibited a local maximum value at a few THz and showed complex behavior beyond 1 THz, corresponding to the skirt region of the local maximum value [11, 19]. In the case of ice, the real dielectric constant ϵ' was almost constant in the range from GHz to sub-terahertz, and it showed complicated behavior beyond 1 THz [11, 14, 19]. This behavior was consistent with the results for a ; thus, we concluded that the local maximum of ϵ'' contributed to the orientation polarization and affected the frequency dependence of a .

Figure 5 shows the frequency dependence of the imaginary dielectric constants ϵ'' of water and heavy water ice over the range of 0.4–1.4 THz at 40, 100, 200, and 240 K. A block of data with error is discarded in Figure 5. As the frequency and temperature increased, ϵ'' increased over the range considered in this chapter. Our ϵ'' values approximately agreed with those reported by Zhang et al. [14] at the same temperature. The frequency range below 1 THz corresponds to the low-frequency tail of the infrared-absorption band of ice; thus, ϵ'' is dominated by the contribution from molecular reorientation. Furthermore, the effect of Debye relaxation may extend to this frequency range. However, the THz range is far from the region dominated by the Debye relaxation. We therefore suggest that in the THz region, the contribution from Debye relaxation which appears in a decrease with increasing frequency is small for ϵ'' . Thus, a simple model for the frequency dependence of ϵ'' is the single term that increases with increasing frequency because it corresponds to the low-frequency tail of the infrared-absorption band at high frequency [11, 14]. Considering previous studies, the equation for ϵ'' in this frequency range is denoted by:

$$\epsilon'' = A\omega^B \quad (8)$$

where the coefficients A and B are temperature-dependent empirical constants. Applying this formula to the results, we obtained values for A and B that gave fitted curves at each

	Water ice		Heavy water ice	
	0.50 THz	1.00 THz	0.50 THz	1.00 THz
$\alpha_{\text{el}} + \alpha_{0,\text{IR}} / \text{\AA}^3$	40.2	40.8	38.0	38.6
$a/\text{\AA}^3 \text{ K}^{-2}$	1.52×10^{-5}	1.15×10^{-5}	2.13×10^{-5}	1.89×10^{-5}

Table 1. Values of $\alpha_{\text{el}} + \alpha_{0,\text{IR}}$, and a derived from fitted curves in Figure 4.

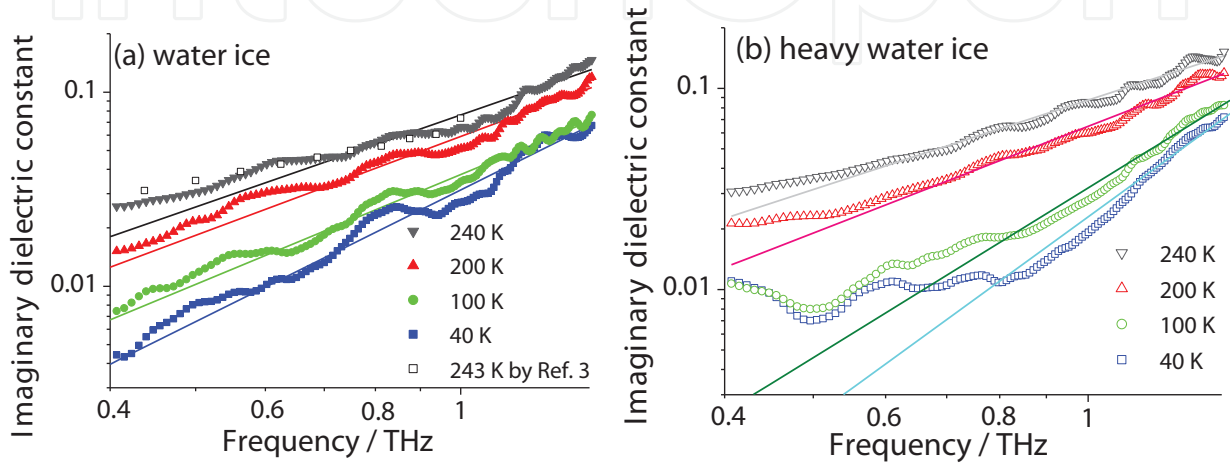


Figure 5. Imaginary dielectric constant ϵ'' of water ice (a) and heavy water ice (b) at four temperatures plotted double logarithmically versus frequency. The solid lines are fitted curves obtained from Eq. (8). The reported data of water ice [14] are plotted in graph (a).

temperature, as shown in **Figure 5**. As the temperature increased, parameter A increased; however, parameter B decreased. This behavior is consistent with that of ice in the GHz range. The fitted curves of heavy water ice are different from the experimental data at low frequency and low temperature (**Figure 5(b)**). This may be caused by experimental uncertainty or events that appear on heavy water ice at low temperatures.

Figure 6 shows the temperature dependence of ϵ'' of both ices from 20 to 240 K at two frequencies. For all four parameters, ϵ'' increased with temperature. According to a previous optical study of ice in the GHz regime, the temperature dependence of ϵ'' in the THz range is determined by the A term in Eq. (8). However, in this chapter, parameters A and B of Eq. (8) showed temperature dependence. We can approximate the temperature dependence of A and B using the least squares method, as follows:

For water ice

$$A = 1.9 \times 10^{-2} + 2.2 \times 10^{-4} \times T \quad \text{in THz}^{-1} (R^2 = 0.954) \quad (9)$$

$$B = 2.3 - 3.1 \times 10^{-3} \times T \quad \text{in THz}^{-1} (R^2 = 0.926) \quad (10)$$

For heavy water ice

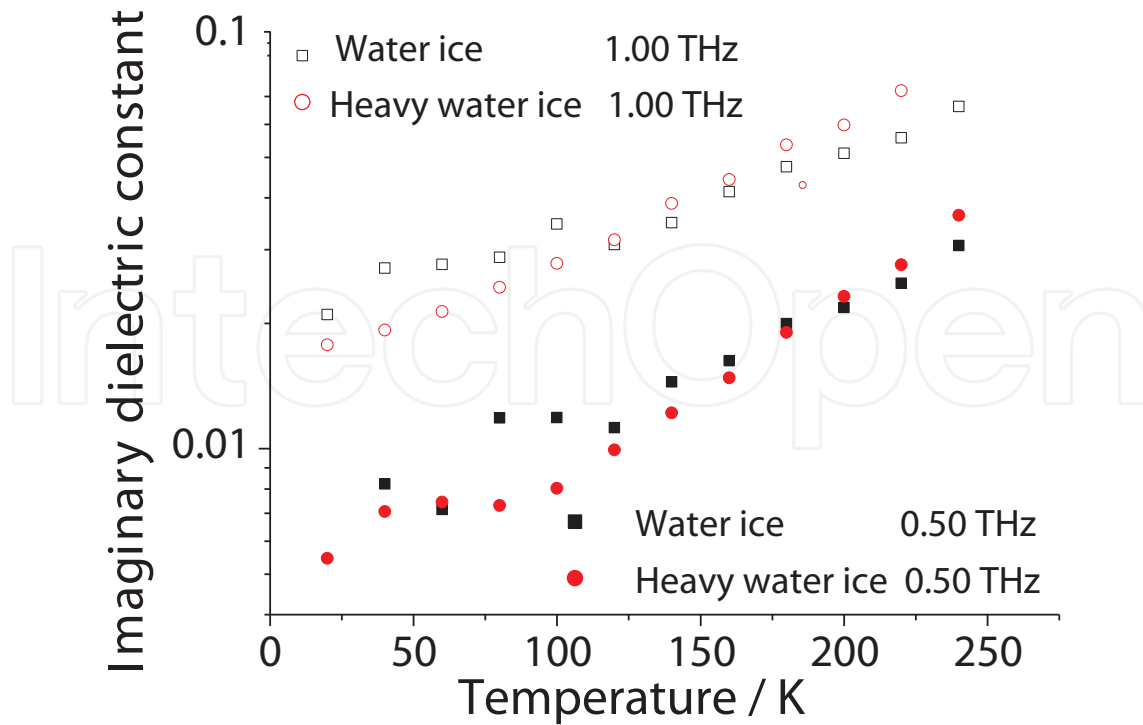


Figure 6. Temperature dependence of the imaginary dielectric constant ϵ'' of water and heavy water ice at 0.50 and 1 THz.

$$A = 5.7 \times 10^{-3} + 3.2 \times 10^{-4} \times T \quad \text{in THz}^{-1} (R^2 = 0.961) \quad (11)$$

$$B = 3.7 - 9.3 \times 10^{-3} \times T \quad \text{in THz}^{-1} (R^2 = 0.997) \quad (12)$$

These formulae fit the experimental results with good agreement, as noted by the correlation coefficients R^2 .

In order to analyze the frequency and temperature dependencies of ϵ'' , approximation of these equations should be considered from the viewpoint of the following factors. For ice, phenomena such as Debye relaxation, acoustic phonon excitation, and infrared phonon absorption are reported in detail in various ways [1, 19, 20]. The dielectric and optical constants of ice material in the THz region may contribute to previous findings. For example, the glass transition of ice at low temperatures is well known. This transition strongly dominates the hydrogen-bond network; thus, information on the dielectric constants of ice over the given temperature range may facilitate astronomy and remote-sensing applications.

4. Dielectric parameters of sulfur hexafluoride hydrate

Figure 7 shows our results for the frequency dependence of the real dielectric constant ϵ' of sulfur hexafluoride hydrate in the range 0.3–1.0 THz at 100.6, 199.9, and 239.9 K. As the frequency increases from 0.3 THz to 1.0 THz, ϵ' increases from 3.02 to 3.09 at 199.9 K. These

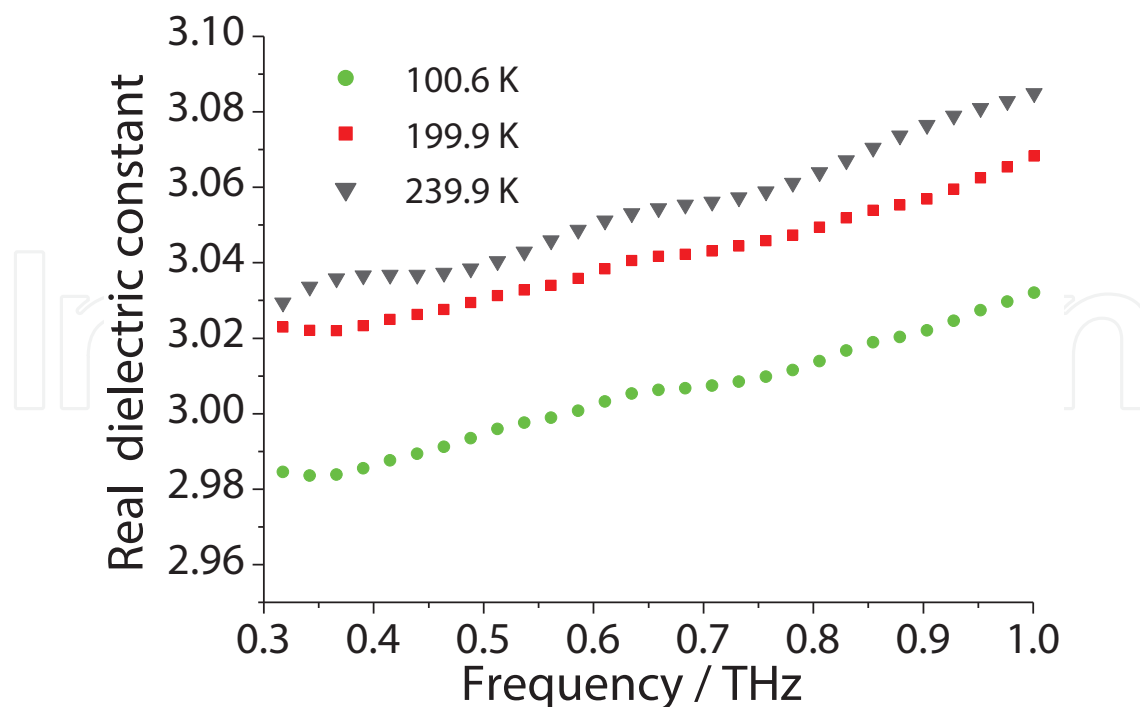


Figure 7. Frequency dependence of real dielectric constant ϵ' of sulfur hexafluoride hydrate at 100.6, 199.9, and 239.9 K.

values are similar to but slightly lower than those for ice under the same conditions [14]. As for the hydrogen-bonded crystal of the water molecules, a lattice vibration significantly contributes to the amplitude of ϵ' in the THz frequency range [14]. Hence, on the basis of a comparison of the ϵ' values, the states of the hydrogen-bonding matrices of ice and gas hydrates, including the nondipolar molecules, are observed to be similar. The difference in the polarizability and the molecular density between ice and the gas hydrate is likely to contribute to a slight difference in these ϵ' values.

According to previous studies, the ϵ' values for ice are constant from 0.1 MHz to 1 THz and show complex behavior beyond 1 THz. The maximum occurs at a few THz [1, 18, 19]. The frequency range of our measurements corresponds to the above range, so we expect that a local maximum for the ϵ' of the gas hydrate exists at a few THz, similar to the local maximum for ice [19].

Figure 8 shows the temperature dependence of the real dielectric constant ϵ' at 0.50, 0.75, and 1 THz. As the temperature increases from 50 to 240 K, ϵ' increases from 3.00 to 3.03 at 500 GHz and from 3.02 to 3.08 at 1 THz. The rate of increase of ϵ' with temperature ($d\epsilon'/dT$) clearly increases beyond 0.75 THz.

Figure 9 shows the frequency dependence of the imaginary dielectric constants ϵ'' of sulfur hexafluoride hydrate in the range 0.3–1.2 THz at 100.6, 199.9, and 239.9 K, together with the reported values for ice [14]. As frequency and temperature increase, ϵ'' increases over the range considered in this chapter. Our ϵ'' values approximately agree with those reported by Zhang et al. for ice at the same temperature [14]. For ice, the frequency range below 1 THz is the low-frequency tail of the infrared-absorption band so ϵ'' is dominated by the contributions from

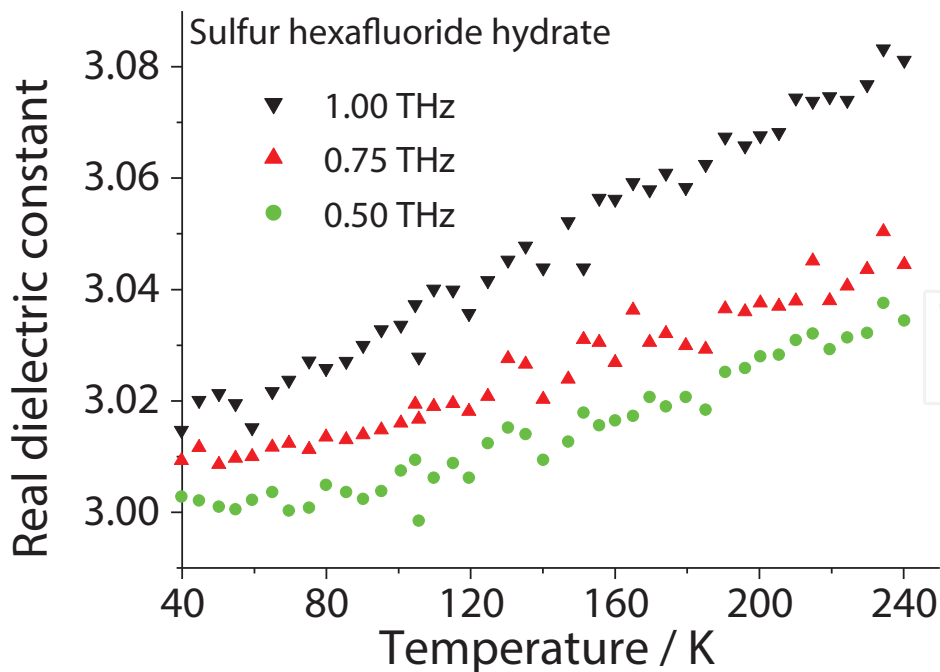


Figure 8. Temperature dependence of the real dielectric constant ϵ' of the sulfur hexafluoride hydrate at 0.50, 0.75, and 1 THz.

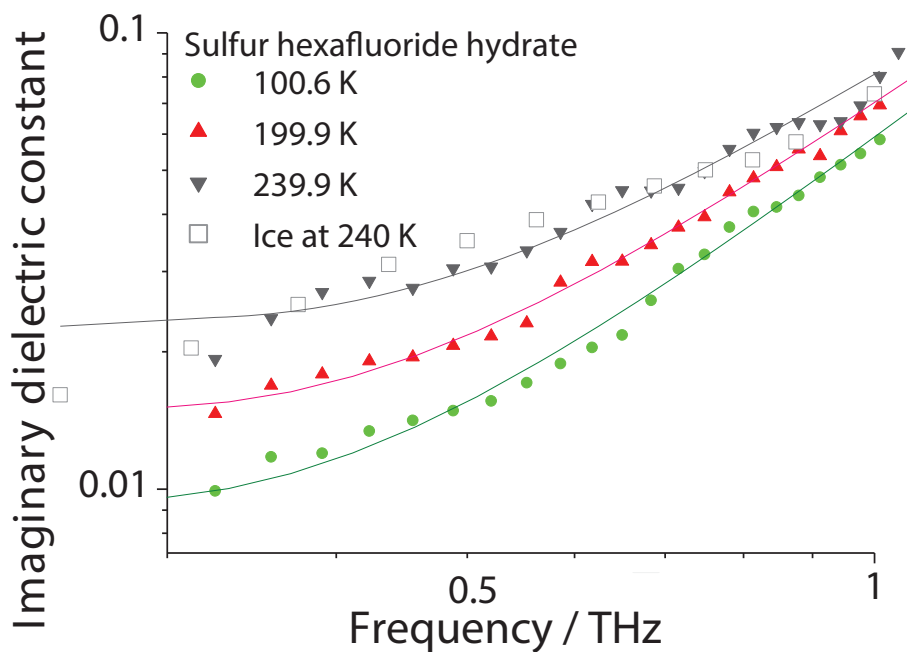


Figure 9. Imaginary dielectric constant ϵ'' of sulfur hexafluoride hydrate at three temperatures plotted double logarithmically versus frequency. The reported values for ice are shown as white squares. The solid lines are fitted curves obtained from Eq. (13).

molecular reorientation. Moreover, the influence of Debye relaxation extends to this frequency range, and thus, a simple model for the frequency dependence of ϵ'' is the sum of two components. One term is contributed by the Debye relaxation and decreases with increasing

frequency. The other term increases with increasing frequency since it is the low-frequency tail of the infrared-absorption band at a high frequency [12, 14, 28]. From previous studies, the equation for ϵ'' in this frequency range is

$$\epsilon'' = (C/\omega) + D\omega^E \quad (13)$$

where the coefficients C , D , and E are temperature-dependent empirical constants. Applying this formula to our results, we obtain the constants C , D , and E , which give the fitted curves at each temperature, as shown in **Figure 9**.

As the temperature increases, parameters C and D increase but parameter E decreases (**Table 2**). This behavior is consistent with that of ice in the GHz range.

Figure 10 shows the temperature dependence of ϵ'' from 50 to 240 K at four frequencies. At all four frequencies, ϵ'' increases with temperature. According to a previous optical study of ice, the temperature dependence of ϵ'' in the THz range is determined by term B in Eq. (13). However, in this chapter, parameters C , D , and E of Eq. (13) all show temperature dependencies. We can approximate the temperature dependencies of C , D , and E using the least squares method, which gives

Temperature (K)	C (THz)	D (THz ⁻¹)	E
10.3	0.00137	0.0474	2.364
100.6	0.00172	0.0574	2.246
200	0.00289	0.0675	2.081
240	0.00477	0.0765	1.894

Table 2. Empirical coefficients C , D , and E obtained via least squares.

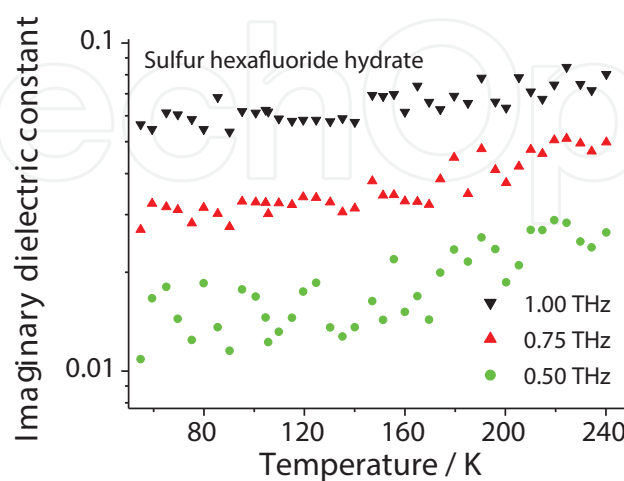


Figure 10. Temperature dependence of the imaginary dielectric constant ϵ'' of sulfur hexafluoride hydrate at 0.50, 075, and 1 THz.

$$C = 1.4 \times 10^{-4} + 3.0 \times 10^{-5} \exp(T \times 2.0 \times 10^{-2}) \quad (14)$$

$$D = 4.6 \times 10^{-2} + 1.2 \times 10^{-4} \times T \quad (15)$$

$$E = 2.4 - 5.8 \times 10^{-2} \exp(T \times 9.1 \times 10^{-3}) \quad (16)$$

The curves fitted using these formulas fit the experimental results with good correlation coefficients R^2 .

To analyze the frequency and temperature dependencies of ϵ'' , we have to consider the approximation of these formulas in terms of the following factors. For ice, phenomena such as Debye relaxation, the excitations of acoustic phonons, and infrared phonon absorption have been reported in detail using various methods [11, 14, 19, 28]. For gas hydrates, there have been few reports for this frequency range. In addition, the structures of gas hydrates are different from those of ice. To investigate the dielectric parameters physically and chemically, we need more information on gas hydrates in this frequency range.

Further, we have to consider the contribution of guest molecules to the polarizability and the properties of the hydrogen bond of the gas hydrate. The hydration number of sulfur hexafluoride hydrate is 17, and the sulfur hexafluoride molecule is nonpolar. We therefore ignored the contribution of guest molecules. In the future, we will carry out a more detailed dielectric study of gas hydrates, including the influence of guest molecules. Nonetheless, since our results in this chapter show a good agreement between the experimental data and the theoretical description, our analysis is reasonably accurate for the investigation of the dielectric behavior of the gas hydrate in the THz frequency range.

5. Temperature dependence of the absorption of tetrahydrofuran

Conversely, the tetrahydrofuran hydrate of the same structure-II of gas hydrate has a broad absorption peak around 0.5 THz (**Figure 11**). This characteristic absorption is not due to the cage structure of the gas hydrate but due to the kinetics of the tetrahydrofuran molecule in the cage or

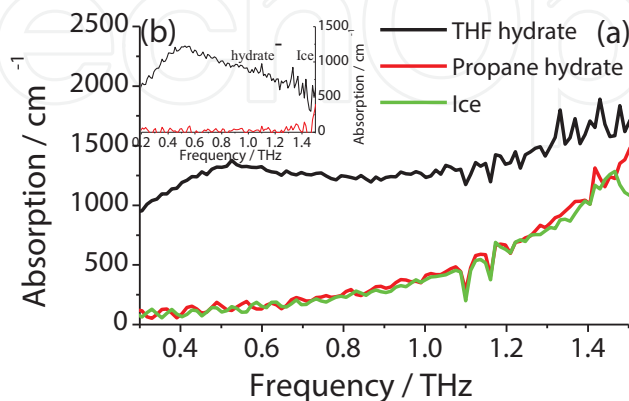


Figure 11. (a) Absorption coefficients of tetrahydrofuran and propane hydrates and ice at 243 K. Inset (b): Subtract spectra of gas hydrates ($\alpha_{\text{hydrate}} - \alpha_{\text{ice}}$).

the interaction between the molecule and the cage. This is because propane hydrate does not exhibit such an absorption peak and the tetrahydrofuran molecule has a larger dipole moment than the propane molecule. A similar absorption peak was found by Klug and Whalley during IR spectroscopy [6]; in their study, tetrahydrofuran hydrate showed two broad absorption peaks at 25 cm^{-1} ($\sim 0.75\text{ THz}$) and 38 cm^{-1} ($\sim 1.14\text{ THz}$) because of rotational oscillations of the tetrahydrofuran molecule at 17 K. Since these absorption peaks are integrated and broadened as the temperature increases due to the reorientation of the tetrahydrofuran molecules and the occupancy of higher-potential minima increases [6], the absorption peak observed in the tetrahydrofuran hydrate probably originates from the rotational oscillations.

6. Summary

We reviewed optical properties of hydrogen-bonded materials that are ice, heavy ice, and gas hydrates within a terahertz frequency and at a wide temperature region of 20–240 K. Frequency and temperature dependencies of the complex dielectric parameter obtained from THz-TDS measurements are described by a mathematical model. An increase in the real part of the dielectric constants with frequency and temperature was observed on all materials.

In terms of the imaginary part of the dielectric parameter of the hydrogen-bonded materials, the THz frequency corresponds to the skirt region of the infrared-absorption band. The imaginary parts of the dielectric parameter of the materials increased with frequency and temperature. The parameters are described by a function of a simple form.

Meanwhile, a gas hydrate which includes polar molecules showed specific absorption at THz frequency. The absorption is based on the rotation of guest molecules inside the structure. Hence THz-TDS can observe the dynamics of molecules in gas hydrates.

Although the optical behavior of the ice and gas hydrates including nonpolar gas molecules was described by a similar model, small but certain differences between ice and gas hydrates were observed on the value of the parameter. The difference corresponds to the difference of the structures; hence, the optical properties in THz frequency provide meaningful information for the hydrogen-bonded materials.

Acknowledgements

This chapter contains many quotes from Refs. [21] and [29]. We thank both journals.

Author details

Kei Takeya* and Kodo Kawase

*Address all correspondence to: takeya@nuee.nagoya-u.ac.jp

Nagoya University, Nagoya city, Aichi, Japan

References

- [1] Petrenko VF, Whitworth RW (2006). *Physics of Ice*. Oxford University Press, Oxford.
- [2] Sloan ED, Koh CA (2007). *Clathrate Hydrates of Natural Gases*, 3rd ed. CRC Press, Boca Raton.
- [3] Ripmeester JA, Tse JS, Ratcliffe CI, Powell BM (1987). A new clathrate hydrate structure. *Nature* 325, 135–136.
- [4] Ohgaki K, Makihara Y, Takano K (1993). Formation of CO₂ hydrate in pure and sea waters. *J. Chem. Eng. Japan* 26, 558–564.
- [5] Takeya S, Honda K, Yoneyama A, Hirai Y, Okuyama J, Hondoh T, Hyodo K, Takeda T (2006). Observation of low-temperature object by phase-contrast x-ray imaging: non-destructive imaging of air clathrate hydrates at 233 K. *Rev. Sci. Instr.* 77, 053705.
- [6] Klug DD, Whalley E (1973). The rotational oscillations of tetrahydrofuran in tetrahydrofuran clathrate hydrate. *Can. J. Chem.* 51, 4062–4071.
- [7] Mak TCW, McMullan RK (1965). Polyhedral clathrate hydrates. X. Structure of the double hydrate of tetrahydrofuran and hydrogen sulfide. *J. Chem. Phys.* 42, 2732–2737.
- [8] Stern LA, Circone S, Kirby SH, Durham WB (2001). Anomalous preservation of pure methane hydrate at 1 atm. *J. Phys. Chem. B* 105, 1756–1762.
- [9] Subramanian S, Kini RA, Dec SF, Sloan ED (2000). Evidence of structure II hydrate formation from methane + ethane mixtures. *Chem. Eng. Sci.* 55, 1981–1999.
- [10] Johari GP, Jones SJ (1976). Infrared polarisability of hexagonal ice. *Nature* 263, 672–673.
- [11] Bertie JE, Labbé HJ, Whalley E (1969). Absorptivity of ice I in the range 4000–30 cm⁻¹. *J. Chem. Phys.* 50, 4501–4520.
- [12] Matsuoka T, Fujita S, Mae S (1996). Effect of temperature on dielectric properties of ice in the range 5–39 GHz. *J. Appl. Phys.* 80, 5884–5890.
- [13] Koh G (1997). Dielectric properties of ice at millimeter wavelengths. *Geophys. Res. Lett.* 24, 2311–2313.
- [14] Zhang C, Lee K-S, Zhang X-C, Wei X, Shen YR (2001). Optical constants of ice Ih crystal at terahertz frequencies. *Appl. Phys. Lett.* 79, 491–493.
- [15] Whalley E, Labbé HJ (1969). Optical spectra of orientationally disordered crystals. III. Infrared spectra of the sound waves. *J. Chem. Phys.* 51, 3120–3127.
- [16] Matzler C, Wegmuller U (1987). Dielectric properties of freshwater ice at microwave frequencies. *J. Phys. D.* 20, 1623–1630.
- [17] Jiang JH, Wu DL (2004). Ice and water permittivities for millimeter and sub-millimeter remote sensing applications. *Atmos. Sci. Lett.* 5, 146–151.

- [18] Takei I, Maeno N (1997). Dielectric low-frequency dispersion and crossover phenomena of HCl-doped ice. *J. Phys. Chem. B.* 101, 6234–6236.
- [19] Warren SG (1984). Optical constants of ice from the ultraviolet to the microwave. *Appl. Opt.* 23, 1206–1225.
- [20] Mishima O, Klug DD, Whalley E (1983). The far infrared spectrum of ice Ih in the range 8–25 cm^{-1} . Sound waves and difference band, with application to Saturn's rings. *J. Chem. Phys.* 78, 6399–6404.
- [21] Takeya K, Fukui T, Takahashi R, Kawase K (2014). Dielectric constants of H_2O and D_2O ice in the terahertz frequency regime over a wide temperature range. *J. Opt.* 16, 094005.
- [22] Gough SR, Hawkins RE, Morris B, Davidson DW (1973). Dielectric properties of some clathrate hydrates of structure II. *J. Phys. Chem.* 77, 2969–2976.
- [23] Davidson DW, Wilson GJ (1963). The low-frequency dielectric properties of ethylene oxide and ethylene oxide hydrate. *Can. J. Chem.* 41, 1424–1434.
- [24] Majid YA, Garg SK, Davidson DW (1968). Dielectric and nuclear magnetic resonance study of the hydrate of sulfur hexafluoride. *Can. J. Chem.* 46, 1683–1690.
- [25] Davies M, Williams K (1968). Dielectric relaxation in clathrates. *Trans. Faraday Soc.* 64, 529–548.
- [26] Davidson DW, Davies MM, Williams K (1964). Dielectric absorption and molecular motion in gas hydrates. *J. Chem. Phys.* 40, 3449–3450.
- [27] Rick SW, Freeman DL (2010). Proton disorder and the dielectric constant of type II clathrate hydrates. *J. Chem. Phys.* 132, 054509.
- [28] Takeya K, Zhang C, Kawayama I, Murakami H, Jepsen PU, Chen J, Wu P, Ohgaki K, Tonouchi M (2009). Terahertz time domain spectroscopy on structure-II gas hydrates. *Appl. Phys. Exp.* 2, 122303.
- [29] Takeya K, Kawayama I, Murakami H, Tonouchi M, Ohgaki K (2011) Dielectric study on gas hydrates using terahertz time domain spectroscopy. In: *Proceedings of the 7th International Conference on Gas Hydrates (ICGH 2011)* 736–742.
- [30] Fletcher NH (1970). *The Chemical Physics of Ice*. Cambridge University Press, 198–246.
- [31] Tonouchi M (2007). Cutting-edge terahertz technology. *Nat. Photonics.* 1, 97–105.
- [32] Yada H, Nagai M, Tanaka K (2008). Origin of the fast relaxation component of water and heavy water revealed by terahertz time-domain attenuated total reflection spectroscopy. *Chem. Phys. Lett.* 464, 166–170.
- [33] Kawase K, Ogawa Y, Watanabe Y, Inoue H (2003). Non-destructive terahertz imaging of illicit drugs using spectral fingerprints. *Opt. Exp.* 11, 2549–2554.
- [34] Song HJ, Nagatsuama T (2011). Present and future of terahertz communications. *IEEE Trans. Terahertz Sci. Technol.* 1, 256–263.

- [35] Duvillaret L, Garet F, Coutaz J-L (1996). A reliable method for extraction of material parameters in terahertz time-domain spectroscopy. *IEEE J. Sel. Top. Quantum Electron.* 2, 739–746.
- [36] Rønne C, Åstrand PO, Keiding SR (1999). THz spectroscopy of liquid H₂O and D₂O. *Phys. Rev. Lett.* 82, 2888–2891.
- [37] Quirico E, Douté S, Schmitt B, Bergh C, Cruikshank DP, Owen TC, Geballe TR, Roush TL (1999). Composition, physical state, and distribution of ices at the surface of triton. *Icarus* 139, 159–178.
- [38] Cruikshank DP, Schmitt B, Roush TL, Owen TC, Quirico E, Geballe TR, Bergh C, Bartholomew MJ, Ore CMD, Douté S, Meier E (2000). Water ice on triton. *Icarus.* 147, 309–316.
- [39] Klinger J (1983). Extraterrestrial ice. A review. *J. Phys. Chem.* 87, 4209–4214.
- [40] Rothery DA (1999). *Satellites of the Outer Planets*, 2nd ed. Oxford University Press, 49–62.
- [41] Mishima O, Calvert LD, Whalley E (1984). ‘Melting ice’ I at 77 K and 10 kbar: a new method of making amorphous solids. *Nature.* 310, 393–395.
- [42] Handa YP, Klug DD (1988). Heat capacity and glass transition behavior of amorphous ice. *J. Phys. Chem.* 92, 3323–3325.

